# Structure and Raman scattering of $Cs_3C_{60}$ under high pressure

S. Fujiki,[1] Y. Kubozono,[1,*] S. Emura,[2] Y. Takabayashi,[1] S. Kashino,[1] A. Fujiwara,[3] K. Ishii,[3] H. Suematsu,[3] Y. Murakami,[4] Y. Iwasa,[5] T. Mitani,[5] and H. Ogata[6]

[1]*Department of Chemistry, Okayama University, Okayama 700-8530, Japan*

[2]*ISIR, Osaka University, Osaka 567-0047, Japan*

[3]*Department of Physics, University of Tokyo, Tokyo 113-0033, Japan*

[4]*KEK-PF, Tsukuba 305-0801, Japan*

[5]*Japan Advanced Institute of Science and Technology, Ishikawa 923-1292, Japan*

[6]*Institute for Molecular Science, Okazaki 444-8585, Japan*

(Received 4 October 1999; revised manuscript received 24 January 2000)

Raman scattering is studied for a pressure-induced superconductor $Cs_3C_{60}$ in a pressure region from 1 bar to 62 kbar. The center frequency $\omega_0$ for $H_g(1)$ and $H_g(2)$ Raman peaks increase by applying pressure, but the increase shows a saturation in the high-pressure region. On the other hand, the $\omega_0$ for $A_g(1)$ and $A_g(2)$ modes increase monotonically in all pressure regions. The electron-phonon coupling constant for $Cs_3C_{60}$ shows a rapid decrease up to 30 kbar and an increase above 30 kbar. This result may be associated with a transformation from a multiphase (body-centered orthorhombic and $A15$ phases) to a single phase around 20 kbar. X-ray powder diffraction pattern at 11 K under a pressure of 40 kbar shows that a superconducting phase for $Cs_3C_{60}$ is body-centered orthorhombic.

In 1995, Palstra *et al.* found that $Cs_3C_{60}$ was a pressure-induced superconductor that exhibited at 14.3 kbar the highest superconducting critical temperature ($T_c = 40$ K) among fullerene superconductors.[1] According to their observation, the $T_c$ appeared by applying pressure and increased with an increase in pressure. This increase in $T_c$ is contrary to the model that a band broadening by applying pressure reduces the density-of-state on the Fermi level, $N(\varepsilon_F)$, and $T_c$ as expected from the BCS theory. One of the explanations for the increase is that the shielding currents are suppressed by a disorder such as fine grain and the two-phase nature of body-centered tetragonal (bct) and $A15$ at 1 bar.[1] Such a disorder may reduce $T_c$ by a fluctuation in the phase of the superconducting order parameter $\Psi$. If only one phase is realized under high pressure, applying pressure should lead to a decrease in the fluctuation of $\Psi$ and improve the superconducting phase. The second explanation is that applying pressure can reduce the phase fluctuation of $\Psi$ and increase the $T_c$ because pressing the grains should improve the connectivity of the material. The third explanation is based on the assumption that $Cs_3C_{60}$ is a Mott-Hubbard insulator. The superconducting transition cannot be expected for an insulating $Cs_3C_{60}$ because all known fullerene superconductors transform to a superconducting state from a metallic state. Applying pressure may change an insulating state to a metallic state, and further a superconducting state.

We studied the structure and physical properties of $Cs_3C_{60}$ at 1 bar by x-ray powder diffraction and ESR (electron spin resonance)[2] and found that $Cs_3C_{60}$ at 1 bar took two phases of body-centered orthorhombic (bco; *Immm*, not bct) as the major phase and $A15$ as the minor phase from 10 to 300 K. It was recently found that $Cs_4C_{60}$ also took a bco structure.[3] No metal-insulator transition was observed for $Cs_3C_{60}$ by ESR from 1.9 to 300 K at 1 bar,[2] suggesting that it is not the Mott–Hubbard insulator. The electron-phonon (e-ph) coupling constant $\lambda$ determined for $Cs_3C_{60}$ from Raman scattering at 1 bar was $\sim 0.18$, which was approximately one third of $Rb_3C_{60}$ and $K_3C_{60}$.[4] The $\lambda$ for $Cs_3C_{60}$ estimated from Raman scattering at 1 bar does not lead to any meaningful $T_c$ in the BCS and McMillan theory, which is consistent with non-superconductivity at 1 bar. In the present paper, we studied the Raman scattering of $Cs_3C_{60}$ from 1 bar to 62 kbar with an interest in the e-ph coupling under high pressure for a pressure-induced superconductor. Further, we studied the crystal structures of $Cs_3C_{60}$ at 101 and 11 K under a pressure of 40 kbar, which corresponds to the normal and the superconducting states, respectively.

The sample of $Cs_3C_{60}$ was prepared by using liquid $NH_3$ at low temperature according to the method reported in Ref. 1. After removing $NH_3$ by pumping under $10^{-3}$ Torr at 100 °C for 18 h and at 140 °C for 1 h, the sample was transferred into a capillary (outer diameter $\phi = 0.7$ mm) and a diamond anvil cell in a glove box for Raman and x-ray diffraction measurements. X-ray diffraction pattern at 298 K and 1 bar was measured with Cu$K\alpha$ radiation (wavelength: 1.5418 Å) by an x-ray diffractometer (Rigaku Rint 1500). X-ray powder diffraction patterns were measured at 11 and 101 K under a pressure of 40 kbar with synchrotron radiation (wavelength: 0.6896 Å) at BL-1B of the Photon Factory in the High Energy Accelerator Research Organization. The Rietveld analyses for x-ray diffraction patterns were achieved by using RIETAN 94 program.[5] The Raman scattering was measured at 298 K with He-Ne laser excitation of 632.8 nm using a Confocal Raman Imaging LabRam system. The center frequency $\omega_0$ the line width $\Gamma$, and the asymmetric parameter $q$ for the Raman peak, were determined by a least-squares fitting with the Breit-Wigner-Fano (BWF) formula. The $H_g(2)$ peaks were analyzed by the three-components fitting, while the $H_g(1)$, $A_g(1)$, and $A_g(2)$ peaks were analyzed by the single-component fitting. The multiple splittings of the $H_g(2)$ mode have been observed in single crystals of $K_3C_{60}$ and $Rb_3C_{60}$.[6] The splittings suggest a lowering of symmetry from Ih for the $C_{60}$ molecule, which is reasonable for the $Cs_3C_{60}$ crystal of *Immm*. The $H_g(1)$ and $H_g(2)$ modes showed a large $1/q$ as observed previously,[4] which reflects the BWF effect. The $A_g(1)$ and $A_g(2)$ peaks showed

 

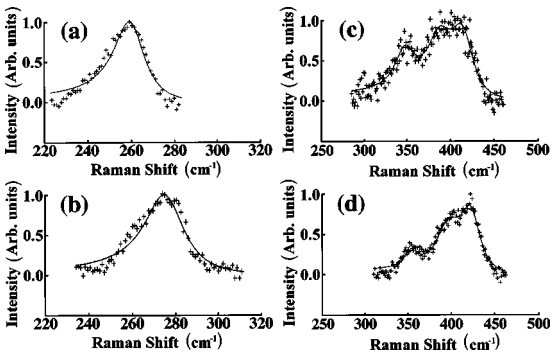


FIG. 1. Raman peaks for the $H_g(1)$ mode at (a) 6 and (b) 47 kbar, and those for the $H_g(2)$ mode at (c) 6 and (d) 47 kbar. The $H_g(1)$ and $H_g(2)$ modes were analyzed by a single BWF and three BWF components, respectively. The crosses and solid lines refer to the experimental and the best-fitted peaks, respectively.

a small $1/q$, i.e., a Lorentzian line shape. The coupling between the phonon and a low-energy continuum ($t_{1u}$-$t_{1u}^*$ interband transition caused by a lowering in symmetry of the $C_{60}$ molecule) is the origin of the BWF effect in the $H_g$ modes.[7]

The $A_g(2)$ Raman peak was observed at $\omega_0$ of 1447 $cm^{-1}$ at 1 bar. The $\omega_0$ value was consistent with those reported previously.[1,2,4] Further, the $\omega_0$ for the $H_g(1)$ (259 $cm^{-1}$) and $A_g(1)$ (493 $cm^{-1}$) modes were consistent with those reported previously.[4] The $\omega_0$ for the $H_g(4)$ peak was 756 $cm^{-1}$, which was close to that in $K_3C_{60}$.[6] The x-ray diffraction pattern at 1 bar was also consistent with that reported previously,[1,2,4] and the Rietveld analysis showed the occupancy of 0.75 for Cs atom. These results support that this sample is $Cs_3C_{60}$.

As a typical example of the Raman scattering in the present study, the $H_g(1)$, $H_g(2)$, $A_g(1)$, and $A_g(2)$ Raman peaks observed at 6 and 47 kbar are shown in Figs. 1 and 2 along with the calculated Raman peaks, in order to show the quality of the Raman data and the validity of the analyses. The Raman data and the analyses in all pressure regions were sufficient to estimate the pressure dependence of the e-ph coupling in $Cs_3C_{60}$. The values of $\omega_0$ and $\Gamma$ for the Raman peaks at 1 bar, 6 kbar, and 47 kbar are collected in Table I.

Figures 3(a) and 3(b) show the pressure dependence of the $\omega_0$ and $\Gamma$ for the $H_g(1)$ peak. The $\omega_0$ increases with an

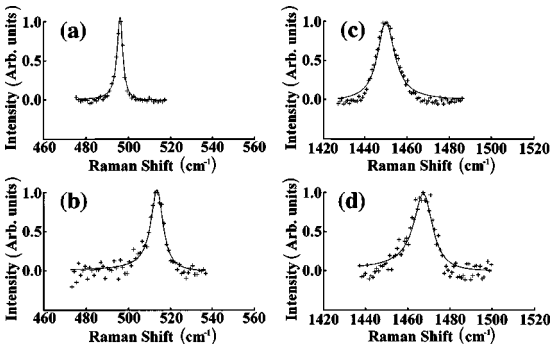


FIG. 2. Raman peaks for the $A_g(1)$ mode at (a) 6 and (b) 47 kbar, and those for the $A_g(2)$ mode at (c) 6 and (d) 47 kbar. Both modes were analyzed by a single BWF component, respectively. The crosses and solid lines refer to the experimental and the best-fitted peaks, respectively.

TABLE I. Values of $\omega_0$ ($cm^{-1}$) and $\Gamma$ ($cm^{-1}$) for the Raman modes at 1 bar, 6 kbar, and 47 kbar.

| Mode | $P$ | $\omega_0$ | $\Gamma$ | $\omega_0$ | $\Gamma$ | $\omega_0$ | $\Gamma$ | $\langle\omega_0\rangle$[a] | $\langle\Gamma\rangle$[a] |
|---|---|---|---|---|---|---|---|---|---|
| $H_g(1)$ | 1 bar | 259 | 8 | | | | | | |
| | 6 kbar | 260 | 9 | | | | | | |
| | 47 kbar | 277 | 11 | | | | | | |
| $H_g(2)$ | 1 bar | 343 | 17 | 372 | 22 | 405 | 22 | 383 | 21 |
| | 6 kbar | 348 | 13 | 387 | 16 | 416 | 17 | 390 | 16 |
| | 47 kbar | 354 | 7 | 396 | 15 | 425 | 15 | 405 | 14 |
| $A_g(1)$ | 1 bar | 493 | 1 | | | | | | |
| | 6 kbar | 496 | 2 | | | | | | |
| | 47 kbar | 514 | 4 | | | | | | |
| $A_g(2)$ | 1 bar | 1447 | 5 | | | | | | |
| | 6 kbar | 1450 | 5 | | | | | | |
| | 47 kbar | 1468 | 6 | | | | | | |

[a]$\langle\omega_0\rangle$ and $\langle\Gamma\rangle$ refer to the weighted average values of $\omega_0$ and $\Gamma$, respectively.

increase in pressure. The rate of increase in $\omega_0$ for applied pressure decreases gradually above 40 kbar. The pressure coefficient $\partial\omega_0/\partial p$ is estimated to be 0.41 $cm^{-1}$/kbar (=4.1 $cm^{-1}$/GPa) for the $\omega_0$ below 40 kbar. This value is larger than that for $C_{60}$, 1.1 $cm^{-1}$/GPa.[8] The $\Gamma$ for the $H_g(1)$ mode increases slightly with an increase in pressure.

The $\omega_0$ of all peaks for the $H_g(2)$ mode increase rapidly with an increase in pressure up to 30 kbar, while the $\omega_0$ saturates above 30 kbar. The pressure dependence of the weighted average value of $\omega_0$ is shown in Fig. 3(c). The pressure dependence is largely different from that in pristine $C_{60}$, in which the $H_g(2)$ mode shows the largest blueshift ($\partial\omega_0/\partial p = 2.4\,cm^{-1}$/GPa) among all modes and a monotonous increase below 60 kbar.[8] The $\Gamma$ of all peaks for the $H_g(2)$ mode in $Cs_3C_{60}$ decrease rapidly with an increase in pressure from 1 bar to 30 kbar, and shows a slight increase above 30 kbar. The pressure dependence of the weighted average value of $\Gamma$ is shown in Fig. 3(d). The weighted average value of $\Gamma$ also decreases rapidly up to 30 kbar and

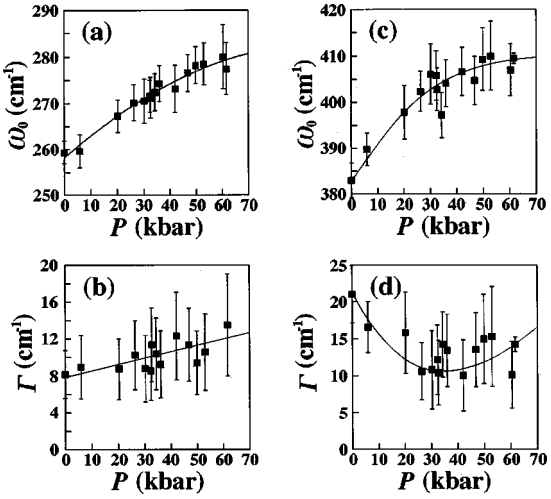


FIG. 3. Pressure dependence of (a) $\omega_0$ and (b) $\Gamma$ for $H_g(1)$ mode, and of the weighted average values of (c) $\omega_0$ and (d) $\Gamma$ in three Raman components for the $H_g(2)$ mode.

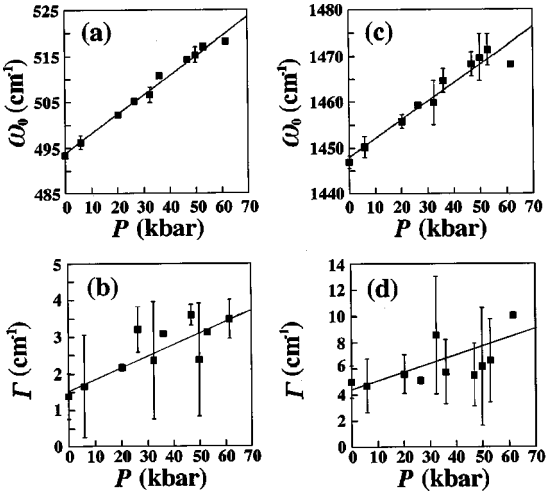


FIG. 4. Pressure dependence of (a) $\omega_0$ and (b) $\Gamma$ for the $A_g(1)$ mode, and of (c) $\omega_0$ and (d) $\Gamma$ for the $A_g(2)$ mode.

increases slightly above 30 kbar. The $q$ values for the $H_g(1)$ and $H_g(2)$ modes are almost constant in all pressure regions.

As seen from Figs. 4(a) and 4(b), the $\omega_0$ and $\Gamma$ for the $A_g(1)$ peak increases linearly with an increase in pressure. The $\partial\omega_0/\partial p$ is estimated to be 0.42 cm$^{-1}$/kbar (=4.2 cm$^{-1}$/GPa), which is extremely larger than that for $C_{60}$ (0.94 cm$^{-1}$/GPa).[8] The $\omega_0$ for the $A_g(2)$ peak also increases linearly with an increase in pressure [Fig. 4(c)]. The $\partial\omega_0/\partial p$ of 0.40 cm$^{-1}$/kbar (=4.0 cm$^{-1}$/GPa) for the $A_g(2)$ peak is consistent with that for the $A_g(1)$ mode, and is larger than that for the $A_g(2)$ mode in $C_{60}$ (1.7 cm$^{-1}$/GPa).[8] The $\Gamma$ increases slightly with an increase in pressure [Fig. 4(d)]. The $q$ values for the $A_g(1)$ and $A_g(2)$ modes are substantially constant in all pressure regions.

The mode–Gruneisen parameters $\gamma[=-(1/\kappa)(1/\omega_0)(d\omega_0/dp)]$ for the $A_g(1)$ and $A_g(2)$ modes are determined from the pressure dependence of $\omega_0$ and the compressibility $\kappa$ $[=(1/V)(dV/dp)]$ to be 0.28 and 9.6 $\times10^{-2}$, respectively; the $\kappa$ is determined to be 3.1 $\times10^{-3}$ kbar$^{-1}$ for $Cs_3C_{60}$.[9] The $\gamma$ for the $A_g(2)$ mode is the same order as that for $C_{60}$ $(6.4\times10^{-2})$.[10] The small $\gamma$ for the $A_g(1)$ and $A_g(2)$ modes suggest that the bond lengths for the $C_{60}$ molecule in $Cs_3C_{60}$ are little affected by the contraction of the crystal lattice under pressure.

The contribution of the $A_g(1)$ and $A_g(2)$ modes to the $\lambda$ in $Cs_3C_{60}$ is extremely small at 1 bar in comparison with the $H_g(1)$ and $H_g(2)$ modes.[4] These modes cannot be expected to contribute to the $\lambda$ even under high pressure. Therefore, the $A_g(1)$ and $A_g(2)$ modes will be affected only by an increase in force constants of the $C_{60}$ molecule caused by applying pressure. The intercalation of three Cs atoms into the $C_{60}$ lattice leads to a softening of the tangential intramolecular $-C_{60}$-$A_g(2)$ mode by $\sim$20 cm$^{-1}$ because of a decrease in force constants of the $C_{60}$ molecule caused by the transfer of three electrons to the antibonding LUMO orbital, i.e., charge-transfer elongation of C–C bonds.[7,11,12] Conversely, as seen from Fig. 4(c), applying pressure of 50 kbar to $Cs_3C_{60}$ leads to a stiffening by 20 cm$^{-1}$, whose variation is comparable to that caused by three-electrons transfer to a LUMO orbital in $C_{60}$.

The $\lambda$ for $Cs_3C_{60}$ can be estimated according to the equation,[7,13–15]

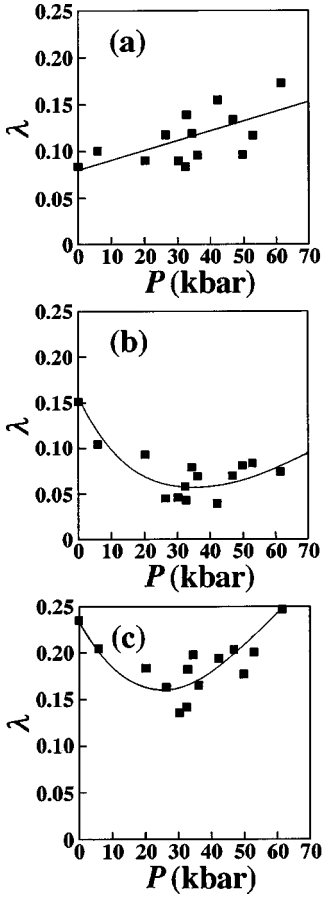


FIG. 5. Pressure dependence of $\lambda$ for (a) $H_g(1)$ and (b) $H_g(2)$ modes, and of (c) total $\lambda$. The $\lambda$ for the $H_g(2)$ mode was estimated from the weighted average values of $\omega_0$ and $\Gamma$.

$$\lambda=\Sigma\lambda_i=\Sigma C\Delta\Gamma_i/[\omega_{01}^2 N(\varepsilon_F)],$$

where $\lambda_i$ is the $\lambda$ for the $i$th mode. $C=d_i/\pi$, $d_i$ being the degeneracy of the $i$th mode ($d=5$ for the $H_g$ mode, $d=1$ for $A_g$ mode). The $\Delta\Gamma_i$ is the difference between the $\Gamma_i$ in $Cs_3C_{60}$ and that in $C_{60}$; the $\Gamma_i$ at 1 bar is employed for $C_{60}$ in all pressure regions. The $N(\varepsilon_F)$ (=9 state eV$^{-1}$C$_{60}^{-1}$ spin$^{-1}$) (Ref. 4) determined at 1 bar is used as the $N(\varepsilon_F)$ in all pressure regions. The $\lambda$ for the $H_g(1)$ and $H_g(2)$ modes at 1 bar are estimated to be 0.08 and 0.15, respectively, and the total $\lambda=0.23$, which is substantially in agreement with that reported previously.[4] The pressure dependence of $\lambda$ for the $H_g(1)$ and $H_g(2)$ modes are shown in Figs. 5(a) and 5(b); the weighted average values of the $\omega_0$ and $\Gamma$ are used in estimating the $\lambda$ from the $H_g(2)$ mode. The $\lambda$ for the $H_g(1)$ mode increases with an increase in pressure, while that for the $H_g(2)$ decreases rapidly from 0.15 to 0.05 up to 30 kbar and increases slightly above 30 kbar. As shown in Fig. 5(c), the total $\lambda$ decreases rapidly up to 30 kbar and increases above 30 kbar. This result may be associated with the phase transition from the multiphase (bco and $A15$) to the single phase (bco) which is found by the pressure-dependent x-ray diffraction study.[1,9] This suggests that a disappearance of disorder in the $Cs_3C_{60}$ crystal plays an important role for a superconductivity.

However, the total $\lambda$ estimated from the $H_g(1)$ and $H_g(2)$ modes is smaller than that ($\sim$0.65) expected from the McMillan formula. We employed the $N(\varepsilon_F)$ at 1 bar in estimat-

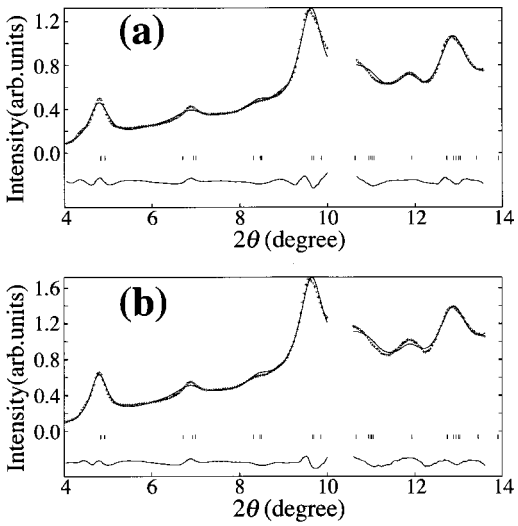


FIG. 6. X-ray diffraction patterns at (a) 101 and (b) 11 K under a pressure of 40 kbar. The crosses and solid lines refer to the experimental and the best-fitted patterns, respectively. Ticks mark the positions of allowed Bragg reflections. The difference between the experimental and the best-fitted patterns is shown by the thin lines in the bottom of each figure.

ing the λ. However, the $N(\varepsilon_F)$ value should decrease with an increase in pressure according to the relation, $N(\varepsilon_F) \sim t_{\text{inter}}^{-1} \sim d_{\text{inter}}^{n}$;[14,15] the parameters, $t_{\text{inter}}$ and $d_{\text{inter}}$, refer to the interatomic hopping integral and the interatomic distance, respectively, and the $n$ is normally 2–3. The unit cell volume $V$ at 30 and 60 kbar can be estimated from the pressure dependence of $V$ for $Cs_3C_{60}$[9] to be ~1540 and ~1410 Å$^3$, respectively. When 3 is adopted for the $n$ in estimating $N(\varepsilon_F)$, the values of $N(\varepsilon_F)$ at 30 and 60 kbar are predicted to be 90 and 85% of that at 1 bar, respectively. When the reduction of $N(\varepsilon_F)$ is taken into account, the λ at 60 kbar should increase from 0.25 to 0.3. The increase in λ is still smaller than that expected by the McMillan formula.

Figures 6(a) and 6(b) show the x-ray powder-diffraction patterns at 101 and 11 K, respectively, under a pressure of 40 kbar. Though the x-ray diffraction pattern measured at 1 bar and 295 K shows the existence of two phases of bco (95%) and $A15$ (5%), no $A15$ phase is observed for both x-ray diffraction patterns at 40 kbar shown in Figs. 6(a) and 6(b). These x-ray diffraction patterns can be indexed with a bco phase ($Immm$): $R_{wp}=3.42\%$ and $R_p=2.76\%$ at 101 K, $R_{wp}=3.23\%$ and $R_p=2.61\%$ at 11 K. The lattice constants $a$, $b$, and $c$ at 11 K under a pressure of 40 kbar are determined to be 11.8(1), 11.32(9), and 11.40(9) Å respectively; the $V$ is 1520(23) Å$^3$. The x-ray diffraction patterns suggest no structural phase transition between 11 and 101 K at 40 kbar, where the superconducting transition should occur. Therefore, it is concluded that the bco phase is the superconducting phase for $Cs_3C_{60}$.

$^1$H NMR spectrum of this sample was measured to identify a stoichiometry of $NH_3$ by a NMR (nuclear magnetic resonance) spectrometer (Bruker DSX400). The $^1$H NMR spectrum shows that the sample contains small amounts of $NH_3$; the stoichiometry is $Cs_3C_{60}(NH_3)_{0.1}$. The $V$ determined from the x-ray diffraction pattern at 1 bar and 295 K, 1654(4) Å$^3$, is in agreement with those reported previously for $Cs_3C_{60}$ within the standard deviation: 1662 Å$^3$ in Ref. 1 and 1659(2) Å$^3$ in Ref. 2. These results suggest that the pressure-induced superconducting $Cs_3C_{60}$ reported in Ref. 1 contains small amounts of $NH_3$. The existence of $NH_3$ in these samples cannot be confirmed from the x-ray diffraction patterns because of extremely small amounts of $NH_3$. The bco phase of $Cs_3C_{60}$ may be stabilized by $NH_3$ occupying the vacancies at $4f$ and $4h$ sites where Cs atoms occupy with the occupancy of 0.75.

In conclusion, the total λ estimated from the $H_g(1)$ and $H_g(2)$ modes also shows a rapid decrease up to 30 kbar and an increase above 30 kbar. This result suggests that a disappearance of the disorder in $Cs_3C_{60}$ crystal leads to an appearance of superconductivity. However, even under high pressure the total λ does not increase to the value (0.65) expected for $Cs_3C_{60}$ by the McMillan formula. The small λ may show the necessity of including other $H_g$ modes and intermolecular vibrations in estimating the e-ph coupling in $Cs_3C_{60}$. The x-ray diffraction patterns at 40 kbar show that the superconducting phase of $Cs_3C_{60}$ is bco as in the case of the normal phase. Further, the $^1$H NMR study suggests that the superconducting phase of $Cs_3C_{60}$ contains small amounts of $NH_3$. The origin of the pressure-induced superconductivity should further be studied.

The authors are grateful to Dr. Hiroshi Kitagawa of JAIST for his valuable suggestion in Raman measurements. The x-ray diffraction study at 40 kbar was performed under a Proposal of KEK-PF (97G201). This study was supported by a Grant-in-Aid (11165227) from the Ministry of Education, Science, Sports and Culture, Japan.

*Corresponding author. Electronic address: kubozono@cc.okayama-u.ac.jp

[1] T. T. M. Palstra *et al.*, Solid State Commun. **93**, 327 (1995).
[2] Y. Yoshida *et al.*, Chem. Phys. Lett. **291**, 31 (1998).
[3] P. Dahlke *et al.*, J. Mater. Chem. **8**, 1571 (1998).
[4] Y. Kubozono *et al.*, Chem. Phys. Lett. **298**, 335 (1998).
[5] F. Izumi, in *The Rietveld Method*, edited by R. A. Young (Oxford University, New York, 1993), p. 236.
[6] J. Winter and H. Kusmany, Phys. Rev. B **53**, 655 (1996).
[7] P. Zhou *et al.*, Phys. Rev. B **48**, 8412 (1993).
[8] D. W. Snoke *et al.*, Phys. Rev. B **45**, 14 419 (1992).
[9] Y. Kubozono *et al.*, in *Electronic Properties of Novel Materials–Science and Technology of Molecular Nanostructures*, Proceedings of the XIII International Winterschool for Electronic Properties of Novel Materials, Austria, 1999, edited by H. Kuzmany *et al.*, AIP Conf. Proc. No. 486 (AIP, New York, 1999), p. 69.
[10] S. H. Tolbert *et al.*, Chem. Phys. Lett. **188**, 163 (1992).
[11] S. J. Duclos *et al.*, Science **254**, 1625 (1991).
[12] K.-A. Wang *et al.*, Phys. Rev. B **45**, 1955 (1992).
[13] C. M. Varma *et al.*, Science **254**, 989 (1991).
[14] M. Schluter *et al.*, Phys. Rev. Lett. **68**, 526 (1992).
[15] K. Prassides *et al.*, in *Fullerene: Status and Perspectives*, edited by C. Taliani, G. Ruani, and R. Zamboni (World Scientific, Singapore, 1992), p. 147.